This is a preprint, the final version is subject to change, of the American Mineralogist (MSA)
Cite as Authors (Year) Title. American Mineralogist, in press.
(DOI will not work until issue is live.) DOI: http://dx.doi.org/10.2138/am-2017-5849

Revision 5

Luogufengite: A new nano-mineral of Fe_2O_3 polymorph with giant coercive field

Huifang Xu[1,*], Seungyeol Lee[1], and Hongwu Xu[2]

[1]NASA Astrobiology Institute, Department of Geoscience, University of Wisconsin–Madison, Madison, Wisconsin 53706, USA

[2]Earth and Environmental Sciences Division, Los Alamos National Laboratory, Los Alamos, NM 87545, USA

* Corresponding author:
Prof. Huifang Xu,
Department of Geoscience,
University of Wisconsin-Madison
1215 West Dayton Street, A352 Weeks Hall
Madison, Wisconsin 53706
Tel: 1-608-265-5887
Fax: 1-608-262-0693
Email: hfxu@geology.wisc.edu

This is a preprint, the final version is subject to change, of the American Mineralogist (MSA)
Cite as Authors (Year) Title. American Mineralogist, in press.
(DOI will not work until issue is live.) DOI: http://dx.doi.org/10.2138/am-2017-5849

ABSTRACT

Luogufengite, Al-bearing ε-Fe_2O_3, is a new member of Fe_2O_3 polymorphs discovered in late Pleistocene basaltic scoria from the Menan Volcanic Complex nearby Rexburg, Idaho. It is an oxidation product of Fe-bearing basaltic glass at high temperature and is associated with maghemite and hematite. Luogufengite is an euhedral or semi-euhedral nano-mineral with its crystal size ranging from ~20 to ~120 nm. The mineral has a space group of $Pna2_1$; its unit-cell parameters refined from synchrotron X-ray powder diffraction pattern are a = 5.0647(3) Å, b = 8.7131(6) Å, c = 9.3842(5) Å, and Z = 4 (calculated density = 4.905 g/cm^3) with the doubled hexagonal (ABAC) packing of oxygen atoms. The eight strongest lines of the measured X-ray diffraction pattern [d(Å)(I)(hkl)] are: 3.197(27.3)(022); 2.945(29.1)(013); 2.708(100)(122); 2.437(35.8)(131); 1.716(24.4)(204); 1.507(40.7)(135); and 1.458(37.2)(330). The empirical formula is $Fe_{1.71}Al_{0.24}Mg_{0.02}Ti_{0.03}O_3$. The crystals display (110) twins with twin boundaries of (110), (100), and (130) due to their pseudo-hexagonal symmetry. Luogufengite is an important mineral that records paleomagnetism of volcanic rocks because of its large magnetic coercivity. This unique magnetic property of the mineral may explain the observed unusually high remanent magnetization in some igneous and metamorphic rocks and even Martian rocks with high remanent magnetization. Some intergrowths of magnetite with ilmenite exsolution lamellae or hematite with magnetite lamellar precipitates have luogufengite-like 2-D crystalline characteristics with the doubled hexagonal packing at the interface between cubic and rhombohedral structures. Luogufengite-like nano-domains at the magnetite / hematite interfaces might be responsible for the large coercive field of lodestones that are partially oxidized magnetite with hematite micro-precipitates.

49 **Keywords**: luogufengite, hematite, maghemite, scoria, nano-mineral, remanent
50 magnetization, coercive field, lodestone

This is a preprint, the final version is subject to change, of the American Mineralogist (MSA)
Cite as Authors (Year) Title. American Mineralogist, in press.
(DOI will not work until issue is live.) DOI: http://dx.doi.org/10.2138/am-2017-5849

INTRODUCTION

The new mineral luogufengite, a Fe_2O_3 polymorph analogous to the synthetic ε-Fe_2O_3, was discovered in late Pleistocene basaltic scoria from the Menan Volcanic Complex nearby Rexburg, Idaho. Powder X-ray diffraction (XRD) and high-resolution transmission electron microscopy (HRTEM) were used to determine its crystal structure and chemical composition. There are five known crystalline polymorphs of Fe_2O_3 to date: hematite (α-Fe_2O_3), maghemite (γ-Fe_2O_3), luogufengite (ε-Fe_2O_3), β-Fe_2O_3 (synthetic) (Zboril et al. 1999), and ζ-Fe_2O_3 (synthetic) (Tucek et al. 2015). Luogufengite is a dark brown nano-mineral — an intermediate polymorph between maghemite and hematite (Tronc et al. 1998; Machala et al. 2011; Lee and Xu 2016). Synthetic ε-Fe_2O_3 phase has a broad range of applications due to its unusual magnetic properties (e.g., giant coercive field, ferromagnetic resonance, and coupled magneto-electrics) (Jin et al. 2004; Gich et al. 2005; Tucek et al. 2010). The coercive field (H_c = 2.0 T) of ε-Fe_2O_3 nano-crystals is much larger than those of oxide-based commercial magnets of $BaFe_{12}O_{19}$ (H_c = 0.64 T) and Co-ferrites (H_c = 0.74 T) (Jin et al. 2004; Kohout et al. 2015).

In this paper, the crystal structure, composition, and mineral association of luogufengite are presented. There is a previous study on the mixture of ε-Fe_2O_3 and magnetite nano-crystals in subcellular phytoferritin of a plant (McClean et al. 2001). However, the published electron diffraction pattern (Figure 2d in the paper) does not support the presence of ε-Fe_2O_3. Herein, we describe a natural ε-Fe_2O_3 (luogufengite) that occurs in basaltic scoria. The name has been approved by Commission on New Minerals, Nomenclature and Classification (CNMNC) of the International Mineralogical Association, (IMA 2016-005) (Xu and Lee 2016). The mineral was named after a Chinese mineralogist, Professor Luo Gufeng (born in 1933), who has passionately taught crystallography and mineralogy at Nanjing University of

China for more than 50 years. Luogufengite has been deposited in the collection of the Geology Museum of the Department of Geoscience, University of Wisconsin-Madison, with specimen numbers UWGM 2341, UWGM 2342, and UWGM 2343.

SAMPLES AND METHODS

Scoria samples containing luogufengite were collected from the Menan Volcanic Complex, Rexburg, Idaho. The Menan Volcanic Complex consists of broad, flat volcanoes, formed by low-viscosity eruptions, with tholeiitic basalts dominating the surface exposures (Hackett and Morgan 1988; Russell and Brisbin 1990). The formation of scoria was related to the interaction of external water with the late-stage (late Pleistocene) eruption in the center of the Menan complex (Hackett and Morgan 1988; Russell and Brisbin 1990). The scoria generally resulted from rapid vesiculation during explosive eruptions of basaltic lava. Luogufengite formed during the formation of scoria at high temperature. Oxidation of Fe-bearing semi-plastic glass at high temperature resulted in the formation of ferric Fe-oxides of luogufengite on surfaces of the vesicles associated with maghemite and hematite (Fig. 1).

The sample for powder X-ray diffraction was carefully scratched off from the vesicles' surfaces within the collected basaltic scoria (Fig. 1). The silicate glass was removed by dissolving the sample in a 10M NaOH solution at 80 °C for 2 days following procedures for enriching synthetic ε-Fe_2O_3 prepared at high temperature (Gich et al. 2006; Namai et al. 2009). The luogufengite crystals were enriched using a weak magnetic bar. Maghemite nano-crystals can be further eliminated by picking up the magnetized portion using an iron needle, because super-paramagnetic maghemite nano-crystals do not have coercive field. High-resolution powder XRD data were collected at beamline 11-BM of the Advanced Photon Source (APS), Argonne National Laboratory. Diffraction patterns were recorded using a

wavelength (λ) of 0.414125 Å. Sample powders were loaded into a Kapton capillary tube that was spun continuously at 5600 rpm during data collection to minimize preferred orientation. Data were collected from 0.5 to 50° 2θ in steps of 0.001° at a scan speed of 0.01°/s. The instrument has a resolution of ~0.007° for the 2θ range used in the structural refinement (2θ: 3° - 25°), based on measured Cagliotti parameters using a LaB_6 standard (NIST SRM 660a) (Supplementary Fig. S1). The X-ray beam size at the sample is ~ 1.5 mm (horizontal) x 0.5 mm (vertical).

The obtained synchrotron XRD data were analyzed using the Rietveld method with the Jade 9.0 program. The starting structural parameters were taken from the study of a synthetic ε-Fe_2O_3 (Gich et al. 2005). A pseudo-Voigt peak-shape function was used for fitting the peak profiles. The peaks at 5.34°-5.41°, 6.79°-6.87°, 8.45°-8.54°, 9.26°-9.34°, 11.65°-11.76° and 14.16°-14.28°) belong to an unknown phase and were thus excluded for the refinement. Our TEM-EDS measurements on luogufengite reveal a total Fe and Al occupancy of $Fe_{3.53}Al_{0.47}$. Previous study on synthetic ε-$Al_xFe_{2-x}O_3$ (Namai et al. 2009) shows that Al prefers the Fe3 and Fe4 sites at ~10 at. %. The ratio of Al occupancies at the Fe3 and Fe4 sites is sensitive to the intensity ratio of $I_{(011)}$ / $I_{(022)}$ of luogufengite, based on simulated XRD patterns. Slight differences in Al occupancies at the Fe3 and Fe sites were determined from matching in the intensity ratio of $I_{(011)}$ / $I_{(022)}$ between the observed and simulated XRD patterns.

Other XRD patterns were collected using a Rigaku Rapid II XRD system (Mo-Kα radiation) in the Geoscience Department, University of Wisconsin - Madison. Diffraction data were recorded on a 2-D image-plate detector. The original two dimensional diffraction rings were then converted to produce conventional 2θ vs. intensity patterns using Rigaku's 2DP software.

HRTEM imaging, X-ray energy-dispersive spectroscopy (EDS), and selected-area

electron diffraction (SAED) analyses were carried out using a Philips CM200-UT microscope equipped with GE light element energy-dispersive X-ray spectroscopy (EDS) at the Materials Science Center at the University of Wisconsin-Madison, and operated at 200 kV. Chemical analyses were obtained using the EDS (spot size 5 with a beam diameter of ~50 nm). Quantitative EDS results were obtained using experimentally determined k-factors from standards of albite, forsterite, anorthite, orthoclase, labradorite, fayalite, and titanite (Hill 2009).

RESULTS AND DISCUSSION

The synchrotron XRD pattern shows that luogufengite is the dominant phase in a treated scoria sample, together with hematite, quartz, hydronium jarosite, and an unknown phase (Fig. 2). A trace amount of calcite originates from the paly-dough that was used for sealing the capillary tube. The XRD data with Mo-Kα radiation also shows a similar pattern, except for the calcite peaks (Supplementary Fig. S2). The (011), (002), (022), (013), (131), (004) and (135) peaks of luogufengite do not overlap with other diffraction peaks from coexisting minerals, although the strongest (122) peak of luogufengite is overlapped with the $(01\bar{4})$ peak of hematite (Fig. 2). The synchrotron XRD pattern of luogufengite shows the broad peaks with a full width at half maximum (FWHM) of ~0.11°, (Table 1), indicating the nanometer sizes of the crystals (Fig. 2). Diffraction peaks from hematite are sharper than those from luogufengite. Likewise, diffraction peaks from quartz are much sharper than peaks from other phases. Diffraction peaks with "?" marks are from an un-identified phase. Its FWHM is very similar to that of hematite (Table 1).

The nano-crystals of luogufengite, maghemite, and hematite were identified using HRTEM, Fast Fourier transform (FFT) patterns, and selected-area electron diffraction (SAED)

patterns (Fig. 3). The diameter of luogufengite ranges from ~20 to ~120 nm (Fig. 3A). Hematite crystals are generally larger than luogufengite crystals, whereas maghemite crystals are smaller than luogufengite crystals (Fig. 3B). HRTEM images show that luogufengite commonly displays {100}, {010}, {00$\bar{1}$}, {011}, and {1$\bar{1}$1} forms (Figs. 3C and 3D). Synthetic ε-Fe_2O_3 crystals similarly display {100}, {01$\bar{1}$} and {011} crystallographic forms (Jin et al. 2004; Lee and Xu 2016). The rod shape of luogufengite is elongated along the ***a***-axis (Fig. 3D). The ideal shape of luogufengite nano-mineral is constructed based on its symmetry and HRTEM images (Fig. 4).

The chemical formulae for luogufengite ($Fe_{1.71}Al_{0.24}Mg_{0.02}Ti_{0.03}O_3$), maghemite ($Fe_{1.69}Al_{0.25}Mg_{0.04}Ti_{0.02}O_3$), and hematite ($Fe_{1.76}Al_{0.02}Mg_{0.03}Ti_{0.19}O_3$) are calculated from X-ray EDS spectra (Fig. 5 and Table 2). The luogufengite and maghemite nano-crystals contain small amounts of Al because the smaller Al^{3+} (compared with Fe^{3+}) prefers the tetrahedral Fe^{3+} site (Namai et al. 2009; Tucek et al. 2010), whereas, co-existing hematite crystals contain small amounts of Ti (Fig. 5 and Table 2).

Large grains of luogufengite have (110) or ($\bar{1}$10) twinning with composition planes of (130) and (100) due to the pseudo-hexagonal symmetry of its crystal structure (Fig. 6A). The relationship between the (110) twins is illustrated in Figures 7A and 7B. The observed twinning is very similar to the (110) twinning in aragonite. The ~120° rotational relationship between (010) and (110) and the displacement along the ***b***/3 are also observed in the luogufengite nano-crystal (Fig. 6B). The relationship is illustrated in Figure 7C. The observed twin relationships are similarly identified in the synthetic ε-Fe_2O_3 crystals (Ding et al. 2007; Lee and Xu 2016).

Rietveld refinement was performed to derive the structural parameters of luogufengite on the basis of the determined space group *Pna2₁* (Gich et al. 2005). Fractional coordinates

and site occupancies are listed in Table 3. The unit cell parameters of luogufengite are very similar to those of synthetic Al-bearing ε-Fe_2O_3 (Fig. 8). The slightly larger ***a*** dimension may be related to a small amount of Mg^{2+} in luogufengite. Table 4 lists the powder XRD data of luogufengite.

The structure of luogufengite contains three octahedra (denoted Fe1, Fe2, and Fe4 sites) and one tetrahedron (denoted as Fe3) (Fig. 9), and the structure is polar, which is associated with its magnetic properties. The average bond distance (1.831 Å) between oxygen and tetrahedral coordinated (Fe, Al) is slightly shorter than that in a synthetic ε-Fe_2O_3 structure (1.879 Å) (Fig. 10). The Fe1 and Fe2 site are shown in the distorted Fe octahedra, whereas the Fe4 sites are less distorted (Fig. 10). These distortions in the Fe sites of luogufengite are responsible for a non-zero orbital component of the total Fe^{3+} magnetic moment (Gich et al. 2005; Tucek et al. 2010).

Luogufengite is a Fe_2O_3 polymorph that is considered as an intermediate phase between maghemite (γ-Fe_2O_3) and hematite (α-Fe_2O_3) (Zboril et al. 2002; Sakurai et al. 2009; Lee and Xu 2016). Oxygen atoms in luogufengite display the doubled hexagonal (ABAC) packing, whereas oxygen atoms in maghemite and hematite have the cubic closest (ABC) and hexagonal (AB) packings, respectively. Specific gravities (g/cm^3) for end-member maghemite, synthetic ε-Fe_2O_3, and hematite are 5.07, 5.01, and 5.27, respectively. Thus, the phase transformations from γ-Fe_2O_3 → ε-Fe_2O_3 and ε-Fe_2O_3 → α-Fe_2O_3 involve changes in packing of oxygen atoms. New experimental results from annealing nontronite at high temperatures indicate that the stability of luogufengite in an amorphous silica matrix is size-dependent (Lee and Xu 2016) (Fig. 11). Sizes of luogufengite crystals may range from ~ 10 to ~ 200 nm in the amorphous silica matrix. Further growth of luogufengite will result in phase transformation to hematite. Synthetic luogufengite was also discovered in ancient

Chinese black-glazed Jian wares, which formed at ~1300°C (Dejoie et al. 2014). Therefore, the formation mechanism of luogufengite suggests a high temperature condition coupled with a fast cooling history, an environment similar to that of an explosive volcanic eruption.

IMPLICATIONS

Luogufengite is an important mineral for understanding the paleomagnetism of volcanic rocks because of its unusual magnetic property. Paleomagnetism requires magnetic minerals to determine Earth's ancient magnetic orientation relative to the magnetic poles at the time of rock formation. Remanent magnetism is detected in some rocks containing magnetic minerals such as magnetite and maghemite. Interestingly, luogufengite could be an important mineral for preserving the remanent magnetic property due to its large magnetic coercivity, the ability to withstand an external magnetic field. Thus, luogufengite is a promising mineral for paleomagnetism studies of volcanic rocks. Ordering of Al in the tetrahedral sites will enhance the magnetic property, because (001) layer with tetrahedra and the (001) layer without tetrahedra have opposite magnetic moments (Tucek et al. 2010; Yoshikiyo et al. 2012).

The mineral with its unique magnetic property may also explain the observed unusually high remanent magnetization in some igneous and metamorphic rocks (Austin et al. 2014; Church et al. 2015; Rajagopalan et al. 1993; Foss and Mckenzie 2011; Schmidt et al. 2007; Kudo et al. 2015), Martian rocks (Acuna et al. 1999), and lodestones (natural magnet). It was proposed that the interface between cubic and rhombohedral phases may play an important role in remanent magnetization (McEnroe et al. 2001, 2002; Robinson et al. 2016). However, the exact role of the interfaces in enhancing this remanent magnetization is still not clear. The Fe-oxide minerals of magnetite with ilmenite exsolution lamellae or hematite with magnetite exsolution lamellae have luogufengite-like 2-D crystals or domains with the doubled

hexagonal packing at the interface between cubic and rhombohedral structures. The luogufengite-like nano-crystals or domains with the giant coercive fields at the interfaces could be an important reason for the unusually high remanent magnetization of some rocks. Lodestones with large remanent magnetization are partially oxidized magnetite intergrown with maghemite and hematite (Banfield et al. 1994; Wasilewski and Kletetschka 1999; Kudo et al. 2015). Hematite lamellae or micro-precipitates in the magnetite host are evident in lodestone (Fig. 12A). Powder X-ray diffraction pattern of lodestone indicates that it is mostly of magnetite with small amount of maghemite and hematite (Fig. 12B). The quantitative analysis of mixture phase is calculated by Rietveld refinement from magnetite (Fleet 2007), maghemite (Shmakov et al. 1995), and hematite (Blake and Hessevick 1966) (Fig. 12B). Stacking faults in magnetite, maghemite and hematite will result in luogufengite-like layer domains with the ABAC stacking locally. Luogufengite-like domains at the magnetite and hematite / ilmenite interfaces are oriented nano-crystals. It is reported that oriented ε–Fe_2O_3 nano-crystals along the ***a***-axis will increase the coercive field when the external magnetic field is parallel to the ***a***-axis (Sakurai et al. 2008). While magnetite and/or maghemite do not have large enough coercive fields (Dunlop and Özdemir 1997), luogufengite-like nano-domains at the magnetite / hematite interfaces might be responsible for the large coercive field of lodestones.

ACKNOWLEDGMENTS

This study was supported by the NASA Astrobiology Institute (N07-5489). Use of the Advanced Photon Source at Argonne National Laboratory was supported by the U. S. Department of Energy, Office of Science, Office of Basic Energy Sciences, under Contract No. DE-AC02-06CH11357. Los Alamos National Laboratory is operated by Los Alamos

243 National Security LLC, under DOE Contract DE-AC52-06NA25396. We also thank Mr.
244 Franklin Hobbs, Dr. Jun Wu, and an anonymous reviewer for providing many helpful
245 suggestions.

246 REFERENCES CITED

247 Acuna, M.H., Connerney, J.E., Ness, N.F., Lin, R.P., Mitchell, D., Carlson, C.W., McFadden,
248 J., Anderson, K.A., Reme, H., Mazelle, C., Vignes, D., Wasilewski, P. and Cloutier, P.
249 (1999) Global distribution of crustal magnetization discovered by the mars global
250 surveyor MAG/ER experiment, Science, 284, 790-793.

251 Austin, J., Hillan, D., Schmidt, P.W., and Foss, C. (2014) Magnetism in the Giles complex.
252 Preview 2014,171, 41-44.

253 Banfield, J.F., Wasilewski, P.J. and Veblen, D.R. (1994) TEM study of relationships between
254 the microstructures and magnetic properties of strongly magnetized magnetite and
255 maghemite. American Mineralogist, 79, 654–667.

256 Blake, R.L and Hessevick, R.E. (1966) Refinement of hematite structure. American
257 Mineralogist, 51, 123-129.

258 Church, N., Austin, J., Schmidt, P.W., and McEnroe, S.A (2015) Rock magnetic properties
259 and mineral microstructure in high-remanence samples from ultramafic intrusions. 26th
260 IUGG General Assembly, 22.06-07.09.15, Prague, Czech Republic.

261 Dejoie, C., Sciau, P., Li, W.D., Noe, L., Mehta, A., Chen, K., Luo, H.J., Kunz, M., Tamura, N.
262 and Liu, Z. (2014) Learning from the past: Rare epsilon-Fe_2O_3 in the ancient black-
263 glazed Jian (Tenmoku) wares. Scientific Reports, 4, 4941.

264 Ding, Y., Morber, J.R., Snyder, R.L. and Wang, Z.L. (2007) Nanowire structural evolution
265 from Fe_3O_4 to epsilon-Fe_2O_3. Advanced Functional Materials, 17, 1172-1178.

266 Dunlop, D.J. and Özdemir, O. (1997) Rock Magnetism: Fundamentals and Frontiers.
267 Combride Studeis in Magnetism Series. 11, P 573. Cambridge University Press, New
268 York.

269 Fleet M.E. (1986) The structure of magnetite: symmetry of cubic spinels. Journal of Solid
270 State chemistry, 62, 75-82.
271 Foss, C., and McKenzie, B. (2011) Inversion of anomalies due to remanent magnetisation: an
272 example from the Black Hill Norite of South Australia, Australian Journal of Earth
273 Sciences: An International Geoscience Journal of the Geological Society of Australia, 58,
274 391–405.
275 Gich, M., Frontera, C., Roig, A., Taboada, E., Molins, E., Rechenberg, H.R., Ardisson, J.D.,
276 Macedo, W.A.A., Ritter, C., Hardy, V., Sort, J., Skumryev, V. and Nogues, J. (2006)
277 High- and low-temperature crystal and magnetic structures of epsilon-Fe_2O_3 and their
278 correlation to its magnetic properties. Chemistry of Materials, 18, 3889-3897.
279 Gich, M., Roig, A., Frontera, C., Molins, E., Sort, J., Popovici, M., Chouteau, G., Marero,
280 D.M.Y. and Nogues, J. (2005) Large coercivity and low-temperature magnetic
281 reorientation in epsilon-Fe_2O_3 nanoparticles. Journal of Applied Physics, 98, 044307.
282 Hackett, W.R. and Morgan, L.A. (1988) Explosive basaltic and rhyolitic volcanism of the
283 eastern Snake River Plain. Guidebook to the Geology of Central and Southern Idaho,
284 Idaho Geological Survey Bulletin, p. 283-301. Wiley, New York.
285 Hill, T.R. (2009) High-resolution transmission electron microscopy investigation of nano-
286 crystals of pyroxene and copper in Oregon sunstones. Master Thesis, University of
287 Wisconsin-Madison.
288 Jin, J., Ohkoshi, S. and Hashimoto, K. (2004) Giant coercive field of nanometer-sized iron
289 oxide. Advanced Materials, 16, 48-51.
290 Kohout, J., Brazda, P., Zaveta, K., Kubaniova, D., Kmjec, T., Kubickova, L., Klemetova, M.,
291 Santava, E. and Lancok, A. (2015) The magnetic transition in ε-Fe_{2O3} nanoparticles:

Magnetic properties and hyperfine interactions from Mössbauer spectroscopy. Jounal of applied physics, 117, 17D505.

Kubo, H., Nakamura, N., Kotsugi, M., Ohkochi, T., Terada, K. and Fukuda, K. (2015) Striped domains of coarse-grained magnetite observed by X-ray photoemission electron microscopy as a source of the high remanence of granites in the Vredefort dome. Frontiers in Earth Science, 3, 31.

Lee, S. and Xu, H. (2016) Size-dependent Phase Map and Phase Transformation Kinetics for Nanometeric Iron(III) Oxides ($\gamma \rightarrow \varepsilon \rightarrow \alpha$ pathway). The journal of physical chemistry C, 120, 13316-13322.

Machala, L., Tucek, J. and Zboril, R. (2011) Polymorphous Transformations of Nanometric Iron(III) Oxide: A Review. Chemistry of Materials, 23, 3255-3272.

McClean, R.G., Schofield, M.A., Kean, W.F., Sommer, C.V., Robertson, D.P., Toth, D. and Gajdardziska-Josifovska, M. (2001) Botanical iron minerals: correlation between nanocrystal structure and modes of biological self-assembly. European Journal of Mineralogy, 13, 1235-1242.

McEnroe, S.A., Harrison, R.J., Robinson, P., Golla, U., and Jercinovic, M.J. (2001) Effect of fine-scale microstructures in titanohematite on the acquisition and stability of natural remanent magnetization in granulite-facies metamorphic rocks, southwest Sweden: Implications for crustal magnetism. Journal of Geophysical Research, 106, 30,523–30,546.

McEnroe, S.A., Harrison, R.J., Robinson, P., and Langenhorst, F. (2002) Nano-scale haematite-ilmenite lamellae in massive ilmenite rock: an example of “lamellar magnetism” with implications for planetary magnetic anomalies. Geophysical Journal International, 151, 890–912.

316 Namai, A., Sakurai, S., Nakajima, M., Suemoto, T., Matsumoto, K., Goto, M., Sasaki, S. and
317 Ohkoshi, S. (2009) Synthesis of an Electromagnetic Wave Absorber for High-Speed
318 Wireless Communication. Journal of the American Chemical Society, 131, 1170-1173.
319 Rajagopalan, S., Schmidt, P.W., and Clark, D.A (1993) Rock magnetism and geophysical
320 interpretation of Black Hill Norite, South Australia. Exploration Geophysics, 24, 209-
321 212.
322 Robison, P., Mcenroe, S.A., Miyajima, N., Fabian, K. and Church, N. (2016) Remanent
323 magnetization, magnetic coupling, and interface ionic configurations of intergrown
324 rhombohedral and cubic Fe-Ti oxides: A short survey. American Mineralogist, 101, 518-
325 530.
326 Russell, W.J. and Brisbin, W.C. (1990) Primary Fractures within a Tuff Cone, North Menan
327 Butte, Idaho, USA. Journal of Volcanology and Geothermal Research, 40, 11-22.
328 Sakurai, S., Namai, A., Hashimoto, K. and Ohkoshi, S. (2009) First Observation of Phase
329 Transformation of All Four Fe_2O_3 Phases (gamma -> epsilon -> beta -> alpha-Phase).
330 Journal of the American Chemical Society, 131, 18299-18303.
331 Schmidt, P.W., McEnroe, S.A., Clark, D.A., and Robinson, P. (2007) Magnetic properties and
332 potential field modeling of the Peculiar Knob metamorphosed iron formation, South
333 Australia: an analog for the source of the intense Martian magnetic anomalies? Journal
334 of Geophysical Research, 112, B03102.
335 Shmakov A. N., Kryukova, G. N., Tsybulya, S. V., Chuvilin, A. L. and Solovyeva, L. P.
336 (1995) Vacancy ordering in gamma-Fe_2O_3–Synchrotron X-ray-powder diffraction and
337 high-resolution microscopy studies. Journal of Applied Crystallography, 28,141-145.
338 Tronc, E., Chaneac, C. and Jolivet, J.P. (1998) Structural and magnetic characterization of
339 epsilon-Fe_2O_3. Journal of Solid State Chemistry, 139, 93-104.

Tucek, J., Machala, L., Ono, S., Namai, A., Yoshikiyo, M., Imoto, K., Tokoro, H., Ohkoshi, S. and Zboril, R. (2015) Zeta-Fe_2O_3 - A new stable polymorph in iron(III) oxide family. Scientific Reports, 5, 15091.

Tucek, J., Zboril, R., Namai, A. and Ohkoshi, S. (2010) epsilon-Fe_2O_3: An Advanced Nanomaterial Exhibiting Giant Coercive Field, Millimeter-Wave Ferromagnetic Resonance, and Magnetoelectric Coupling. Chemistry of Materials, 22, 6483-6505.

Wasilewski, P. and Kleteschka, G. (1999) Lodestone: Natures only permanent magnet-What it is and how it gets charged. Geophysical research letters, 26, 2275-2278.

Yoshikiyo, M., Yamada, K., Namai, Asuka. and Ohkoshi, S. (2014) Study of the Electronic Structure and Magnetic Properties of ε-Fe_2O_3 by First-Principles Calculation and Molecular Orbital Calculations. The journal of physical chemistry C, 116, 8688-8691.

Xu, H. and Lee, S. (2016) Luogufengite, IMA 2016-005. CNMNC Newsletter No. 31 (June 2016), page 695; Mineralogical Magazine, 80: 691–697.

Zboril, R., Mashlan, M., Krausova, D. and Pikal, P. (1999) Cubic beta-Fe_2O_3 as the product of the thermal decomposition of $Fe^{-2}SO_4^{+3}$. Hyperfine Interactions, 120, 497-501.

Zboril, R., Mashlan, M. and Petridis, D. (2002) Iron(III) oxides from thermal processes-synthesis, structural and magnetic properties, Mossbauer spectroscopy characterization, and applications. Chemistry of Materials, 14, 969-982.

FIGURE CAPTIONS

Figure 1. (A) A scoria hand specimen showing the porous texture with vesicles covered by reddish and brownish Fe-oxides of luogufengite, hematite and maghemite. (B) A polished surface of a scoria thin section shows coating of the oxides on the vesicles' surfaces. Glassy groundmass of the scoria contains crystals of magnetite and platy labradorite minerals. The image was recorded under the reflected light mode.

Figure 2. The synchrotron XRD pattern shows diffraction peaks from luogufengite (dominant), hematite, quartz, hydronium jarosite, and an un-identified phase. Diffraction peaks from luogufengite, hematite, quartz and hydronium jarosite are marked below the XRD pattern. Percentages of these phases were calculated using the Rietveld method. A trace amount of calcite is from the platy-dough used for sealing the capillary tube. Peaks with "?" marks are from an un-identified phase. Their peak width (FWHM) is very similar to that of hematite. The refinement was conducted using the XRD pattern with the peaks from the unknown phase removed. The residual between measured and calculated patterns is illustrated right below the XRD pattern.

Figure 3. (A) Bright-field TEM images showing aggregated luogufengite with an inserted SAED pattern, (B) Bright-field TEM image shows that hematite crystals are generally lager than luogufengite, whereas maghemite crystals are generally smaller than luogufengite, (C) An HRTEM image and its FFT pattern (inserted at the up-right corner) showing single luogufengite nano-crystals from the outlined area in Figure 3B, (D) An HRTEM image of the rod-shape of luogufengite elongated along the ***a***-axis.

Figure 4. Proposed ideal morphology for luogufengite nano-mineral based on HRTEM images.

Figure 5. Representative X-ray EDS spectra from (A) maghemite, (B) luogufengite and

(C) hematite nano-minerals. Cu peaks are from the lacey carbon-coated copper grid that holds the TEM specimen.

Figure 6. (A) An HRTEM image showing the luogufengite in a (110) twinning relationship. The composition plans are (130) and (100) due to its pseudo-hexagonal structure. The [311] zone-axis from one crystal is parallel to the [021] zone-axis of its twined crystal. (B) An HRTEM image showing the composition plane boundaries between (110) and (010) of luogufengite and a stacking fault in a right side crystal.

Figure 7. (A) Structure model showing the (011) twin relationship between the neighboring nano-crystals along the ***c***-axis in Figure 6A. (B) Stereogram showing axial relationship between the twined crystals in Figure 6. Red dots correspond to the axes of the right crystal in the model. Blue dots correspond to the axes of the center crystal in the model. (C) Structure model for Figure 6B showing ~120° rotation twin relationship with the displacement of ***b***/3.

Figure 8. Comparisons of unit cell parameters of luogufengite (black circle) and synthetic Al-bearing ε-Fe_2O_3 (red squares) (Namai et al. 2009).

Figure 9. Polyhedral models showing the crystal structure of luogufengite.

Figure 10. Bond distances for the polyhedra in synthetic pure ε-Fe_2O_3 (Gich et al. 2006) and luogufengite. The tetrahedra in the natural phase are slightly smaller than those in synthetic ε-Fe_2O_3.

Figure 11. A size-dependent phase map of iron (III) oxide polymorphs (Modified from Lee and Xu 2016).

Figure 12. (A) A hand sample and optical microscope image of lodestone from Utah showing hematite lamellae in the magnetite host. The image was recorded under reflected light mode. (B) XRD pattern from the lodestone thin section. Percentages of mineral phases

406 were calculated using the Rietveld method. The residual between the measured and calculated
407 profiles is illustrated right below the XRD pattern.

Table 1. The d-values, intensities and FWHMs of selected peaks (*hkl*) as well as crystallite size/strain analyses of observed minerals in the vesicles' coating layers.

Phase	(h k l)	d(Å)	I_{obs}	FWHM 2 (°)
	(0 1 1)	6.387	3.657	0.106(5)
Luogufengite	(0 0 2)	4.694	3.752	0.099(4)
	(0 2 2)	3.196	7.922	0.098(6)
Crystallite size (nm) = 38.8(4.9) and strain (%) = 0.102(55)				
	(0 1 2)	3.673	14.575	0.034(4)
Hematite	(1 1 3)	2.2	13.117	0.035(7)
	(1 1 6)	1.689	21.592	0.039(5)
Crystallite size (nm) = 107.7(24.5) and strain (%) = 0.042(33)				
	(0 1 0)	4.256	20.108	0.011(4)
Quartz	(0 1 1)	3.343	100	0.013(6)
	(2 1 1)	1.542	14.021	0.013(5)
Crystallite size (nm) = 832.5(109.1) and strain (%) = 0.027(5)				
Hydronumum jasosite	(0 1 2)	5.105	6.262	0.021(3)
		4.42	14.305	0.029(1)
Unknown		3.487	2.564	0.031(3)
		2.795	10.567	0.034(2)

Unit cell parameters for quartz: a_h = 4.91532(8), c_h = 5.40604(11) Å;
for hematite: a_h = 5.02217(7), c_h = 13.70852(27) Å;
for hydronium jarosite: a_h = 7.2916(1), c_h = 17.5571(4) Å.
The instrumental resolution: 0.007° (see supplementary Fig. S1 for details).

Table 2. Chemical compositions of luogufengite, maghemite, and hematite.

Luogufengite	(1)	(2)	(3)	(4)	(5)	Average
Fe_2O_3 (wt.%)	90.03%	89.74%	89.76%	90.18%	90.01%	89.94%
Al_2O_3	7.84%	8.68%	8.01%	7.62%	7.48%	7.93%
MgO	1.06%	1.06%	1.73%	0.80%	1.46%	1.22%
TiO_2	1.07%	0.52%	0.50%	1.40%	1.05%	0.91%
Fe	1.70	1.70	1.71	1.71	1.71	1.71
Al	0.23	0.26	0.24	0.23	0.22	0.24
Mg	0.02	0.02	0.03	0.02	0.03	0.02
Ti	0.05	0.02	0.02	0.04	0.04	0.03
Average chemical formula: $Fe_{1.71}Al_{0.24}Mg_{0.02}Ti_{0.03}O_3$						
Maghemite	(1)	(2)	(3)	(4)	(5)	Average
Fe_2O_3 (wt.%)	88.04%	88.37%	89.41%	89.13%	89.54%	88.90%
Al_2O_3	9.43%	8.36%	7.87%	8.44%	8.59%	8.54%
MgO	2.14%	2.50%	2.33%	2.14%	1.62%	2.14%
TiO_2	0.39%	0.77%	0.39%	0.29%	0.25%	0.42%
Fe	1.67	1.68	1.71	1.70	1.70	1.69
Al	0.28	0.25	0.24	0.25	0.26	0.25
Mg	0.04	0.05	0.04	0.04	0.03	0.04
Ti	0.01	0.03	0.01	0.01	0.01	0.02
Average chemical formula: $Fe_{1.69}Al_{0.25}Mg_{0.04}Ti_{0.02}O_3$						
Hematite	(1)	(2)	(3)	(4)	(5)	Average
Fe_2O_3 (wt.%)	92.85%	92.89%	92.71%	93.32%	93.04%	92.96%
Al_2O_3	1.10%	0.42%	0.29%	0.78%	0.76%	0.67%
MgO	1.28%	1.20%	1.98%	1.09%	1.53%	1.42%
TiO_2	4.77%	5.49%	5.02%	4.81%	4.67%	4.95%
Fe	1.76	1.76	1.76	1.77	1.77	1.76
Al	0.03	0.01	0.01	0.02	0.02	0.02
Mg	0.02	0.02	0.04	0.02	0.02	0.03
Ti	0.18	0.21	0.19	0.18	0.18	0.19
Average chemical formula: $Fe_{1.76}Al_{0.02}Mg_{0.03}Ti_{0.19}O_3$						

Notes: All calculations are based on 3-oxygen basis.

This is a preprint, the final version is subject to change, of the American Mineralogist (MSA)
Cite as Authors (Year) Title. American Mineralogist, in press.
(DOI will not work until issue is live.) DOI: http://dx.doi.org/10.2138/am-2017-5849

Table 3. Atomic coordinates of luogufengite

Space group $Pna2_1$				
Atom	Occupancy	x	y	z
Fe1	Fe 1.00	0.1941(3)	0.1569(4)	0.5789(6)
Fe2	Fe 1.00	0.6844(5)	0.0228(3)	0.7893(7)
Fe3	Fe 0.73 Al 0.27	0.1878(3)	0.1531(6)	0.0000(2)
Fe4	Fe 0.80 Al 0.20	0.8081(4)	0.1602(2)	0.3044(6)
O1	O 1.00	0.9812(3)	0.3356(3)	0.4396(5)
O2	O 1.00	0.5106(2)	0.4953(3)	0.4154(5)
O3	O 1.00	0.6477(3)	0.9869(7)	0.1961(6)
O4	O 1.00	0.1569(5)	0.1568(6)	0.1902(3)
O5	O 1.00	0.8325(5)	0.1705(4)	0.6651(3)
O6	O 1.00	0.5391(4)	0.1717(2)	0.9423(6)

Lattice parameters: a = 5.0647(3), b= 8.7131(6), c = 9.3842(5)
Refinement agreement parameter: R = 9.35%

This is a preprint, the final version is subject to change, of the American Mineralogist (MSA)
Cite as Authors (Year) Title. American Mineralogist, in press.
(DOI will not work until issue is live.) DOI: http://dx.doi.org/10.2138/am-2017-5849

Table 4. Powder XRD data for luogufengite*

I_{obs}	d_{obs}	d_{clac}	I_{clac}	*hkl*	I_{obs}	d_{obs}	d_{clac}	I_{clac}	*hkl*
7.6	6.3873	6.3852	9.4	0 1 1			1.9840	4.1	2 2 2
2.1	4.6944	4.6921	1.5	0 0 2	16.8	1.9727	1.9758	8.8	0 4 2
1.7	3.9694	3.9680	3.9	1 1 1			1.9682	3.7	2 0 3
4.8	3.3033	3.3028	6.1	1 2 0			1.9622	10.2	1 3 3
27.3	**3.1965**	3.2013	7.8	1 1 2	7.3	1.9167	1.9199	10.6	2 1 3
		3.1926	27.0	0 2 2	6.1	1.8386	1.8407	7.4	1 4 2
4.1	3.1167	3.1155	2.5	1 2 1			1.8348	2.8	0 1 5
29.1	**2.9445**	2.9441	35.4	0 1 3	2.8	1.7912	1.7937	3.5	2 2 3
100.0	**2.7082**	2.7745	1.3	0 3 1			1.7251	1.0	1 1 5
		2.7008	100.0	1 2 2	**24.4**	**1.7155**	1.7210	13.4	2 0 4
40.6	**2.5343**	2.5453	15.7	1 1 3			1.7170	7.8	1 3 4
		2.5324	19.2	2 0 0			1.7133	3.1	0 5 1
		2.5195	6.9	1 3 0	6.9	1.5594	1.5628	6.5	3 1 2
35.8	**2.4369**	2.4449	11.2	2 0 1			1.5577	2.9	2 4 2
		2.4333	31.1	1 3 1	10.8	1.5208	1.5223	10.7	0 5 3
		2.4317	3.1	2 1 0	**40.7**	**1.5069**	1.5079	12.7	2 0 5
4.1	2.3421	2.3461	6.6	0 0 4			1.5051	36.7	1 3 5
7.8	2.2731	2.2711	7.9	1 2 3			1.4598	24.9	3 3 0
14.5	2.2231	2.2285	5.9	2 0 2	**37.2**	**1.4582**	1.4596	2.0	2 4 3
		2.2197	14.9	1 3 2			1.4528	12.1	0 6 0
2.9	2.1793	2.1783	2.9	0 4 0	11.4	1.4051	1.4062	8.7	3 2 3
12.4	2.1558	2.1590	15.0	2 1 2			1.3959	1.6	1 6 0
1.9	2.0050	2.0011	2.9	1 4 0	7.7	1.3715	1.3728	8.1	2 5 2
					8.6	1.3028	1.3047	6.4	2 5 3

*Bold values are for the eight strongest peaks.

This is a preprint, the final version is subject to change, of the American Mineralogist (MSA)
Cite as Authors (Year) Title. American Mineralogist, in press.
(DOI will not work until issue is live.) DOI: http://dx.doi.org/10.2138/am-2017-5849

Fig. 1

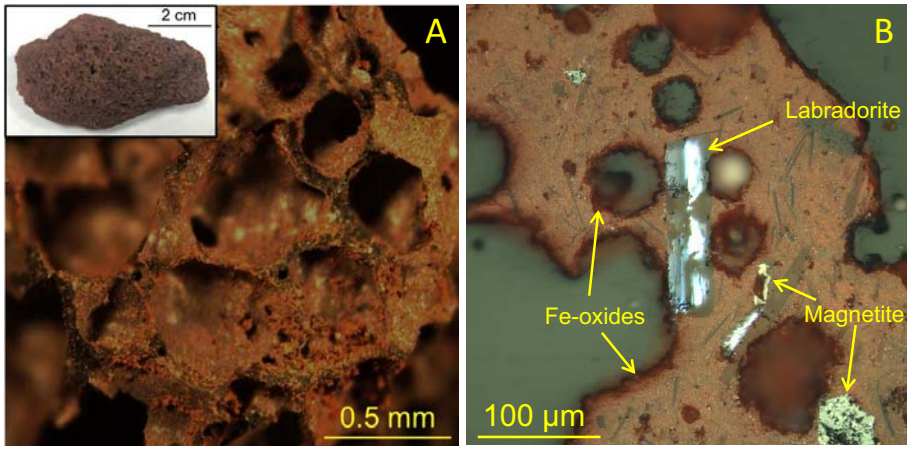

This is a preprint, the final version is subject to change, of the American Mineralogist (MSA)
Cite as Authors (Year) Title. American Mineralogist, in press.
(DOI will not work until issue is live.) DOI: http://dx.doi.org/10.2138/am-2017-5849

Fig. 2

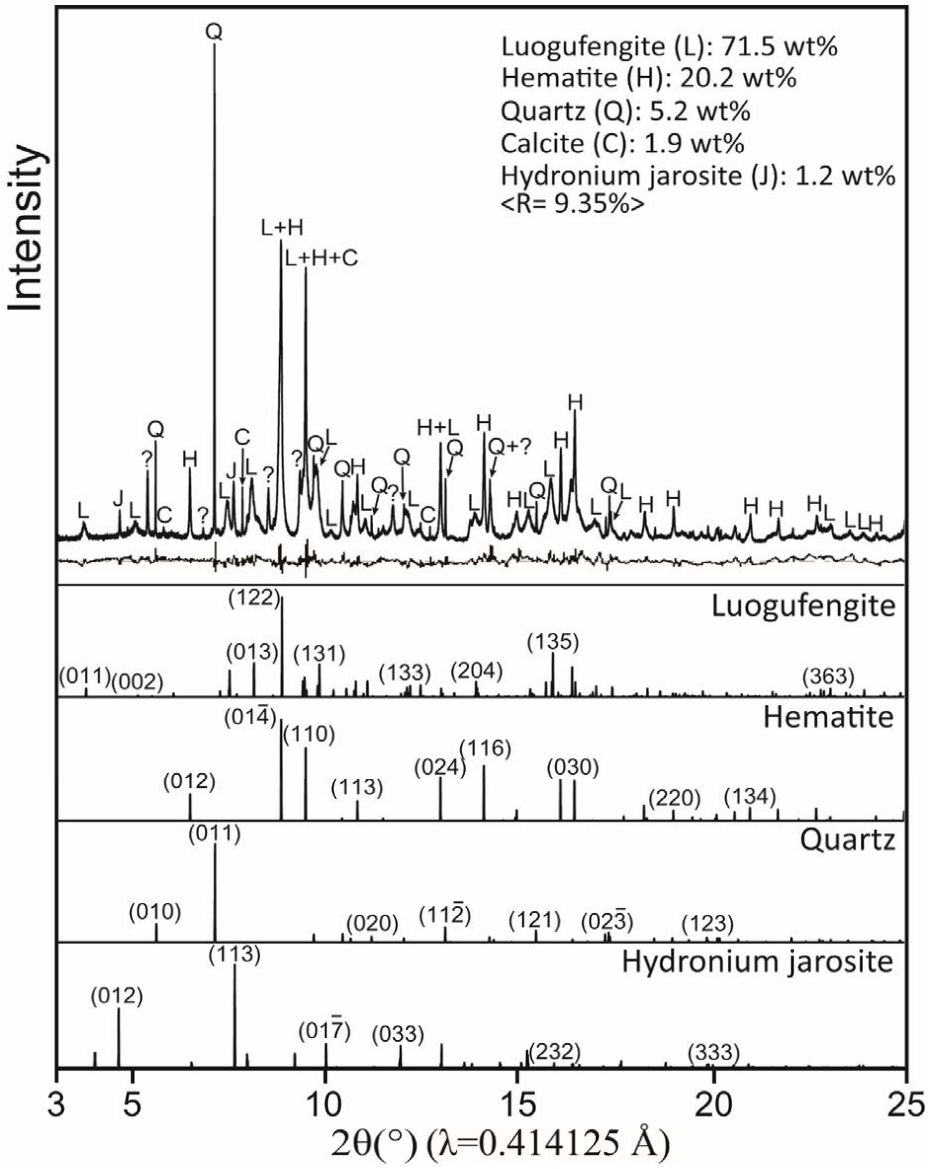

This is a preprint, the final version is subject to change, of the American Mineralogist (MSA)
Cite as Authors (Year) Title. American Mineralogist, in press.
(DOI will not work until issue is live.) DOI: http://dx.doi.org/10.2138/am-2017-5849

Fig. 3

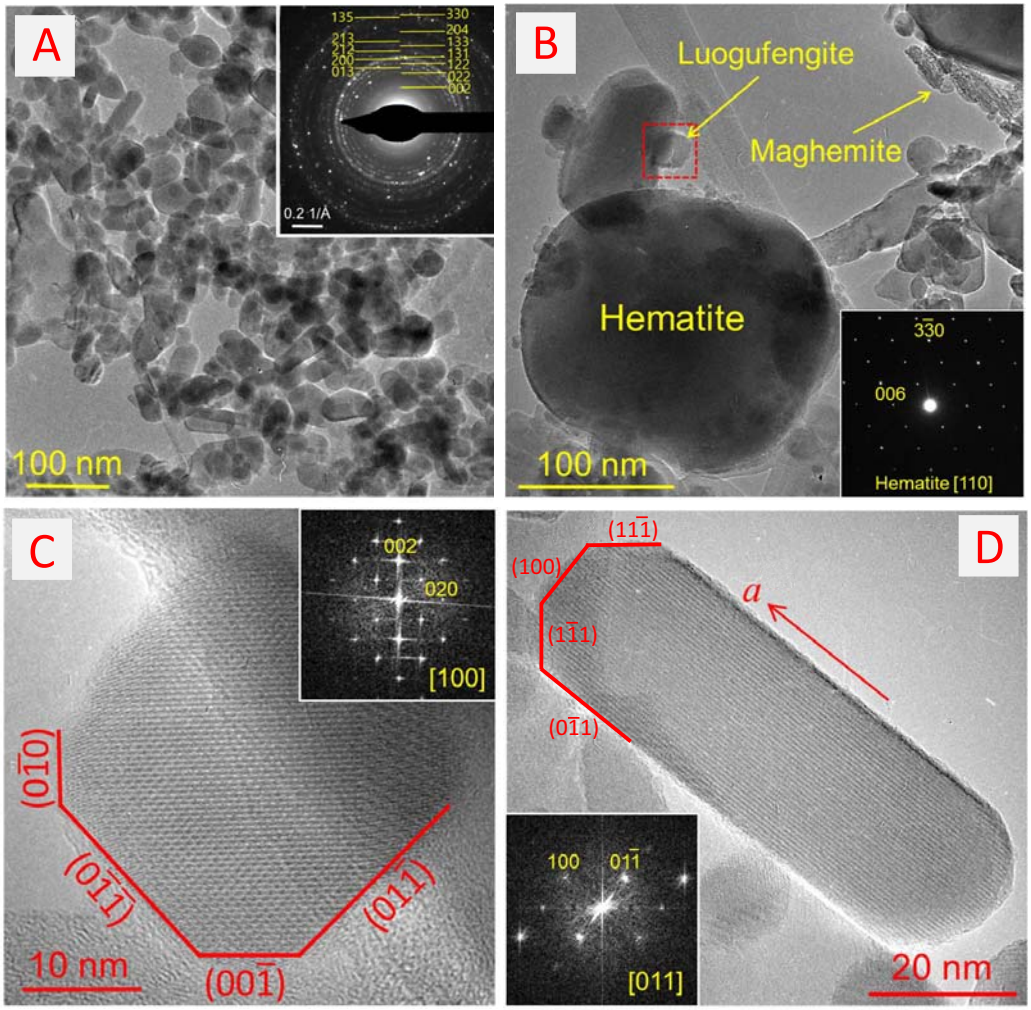

This is a preprint, the final version is subject to change, of the American Mineralogist (MSA)
Cite as Authors (Year) Title. American Mineralogist, in press.
(DOI will not work until issue is live.) DOI: http://dx.doi.org/10.2138/am-2017-5849

Fig. 4

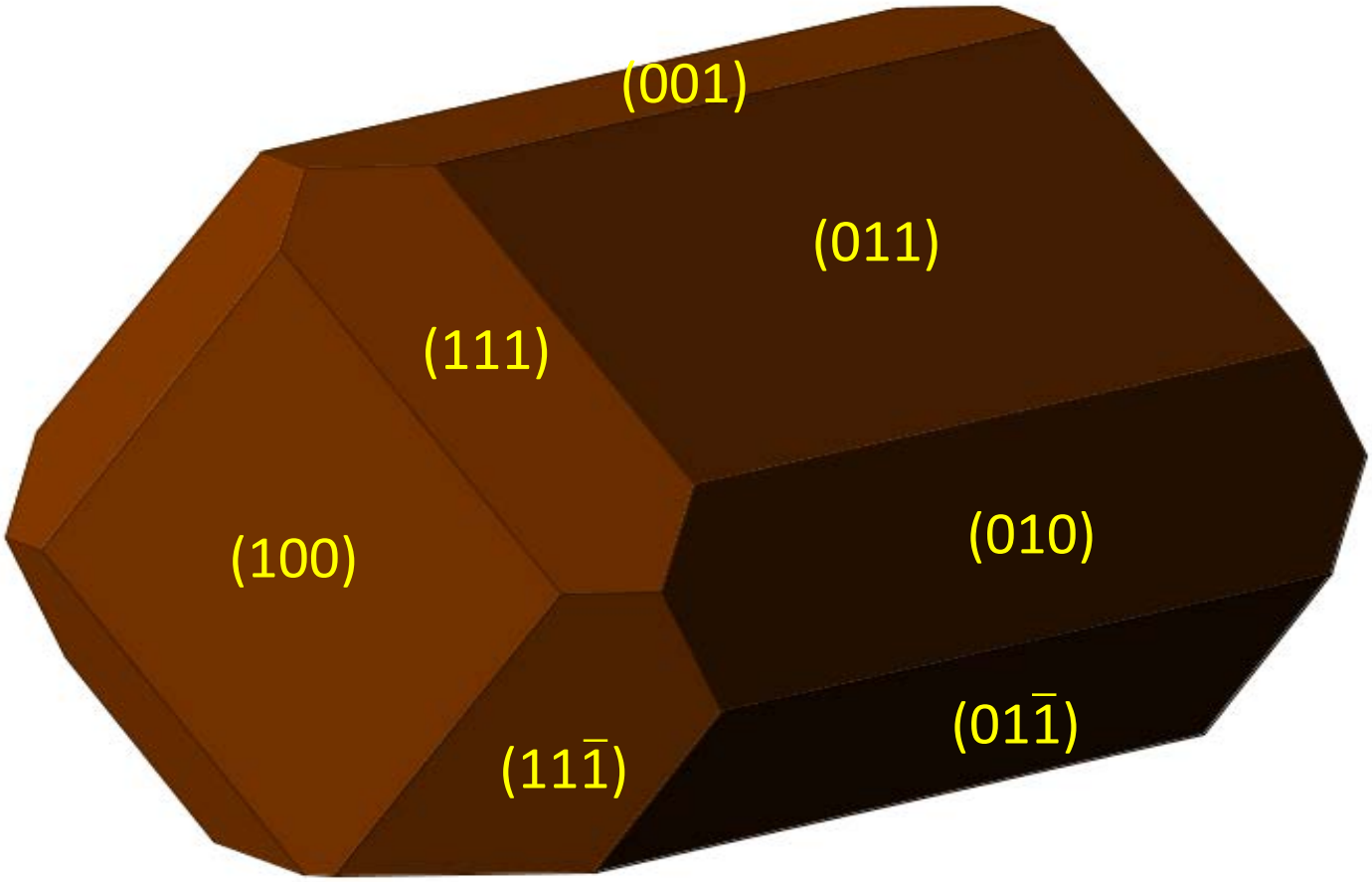

This is a preprint, the final version is subject to change, of the American Mineralogist (MSA)
Cite as Authors (Year) Title. American Mineralogist, in press.
(DOI will not work until issue is live.) DOI: http://dx.doi.org/10.2138/am-2017-5849

Fig. 5

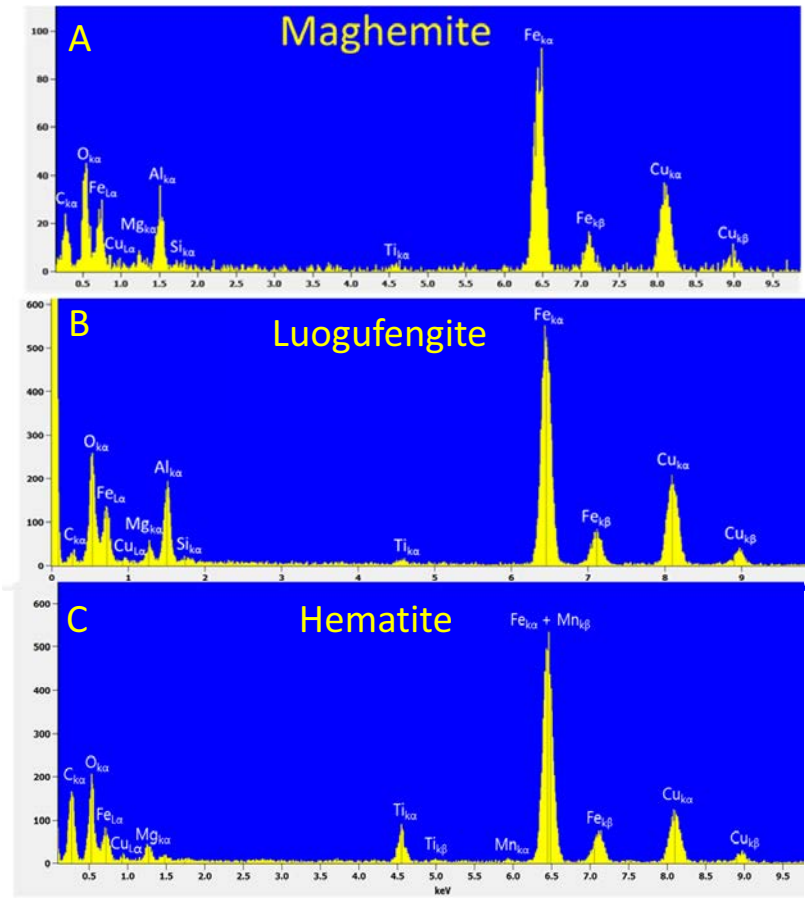

This is a preprint, the final version is subject to change, of the American Mineralogist (MSA)
Cite as Authors (Year) Title. American Mineralogist, in press.
(DOI will not work until issue is live.) DOI: http://dx.doi.org/10.2138/am-2017-5849

Fig. 6

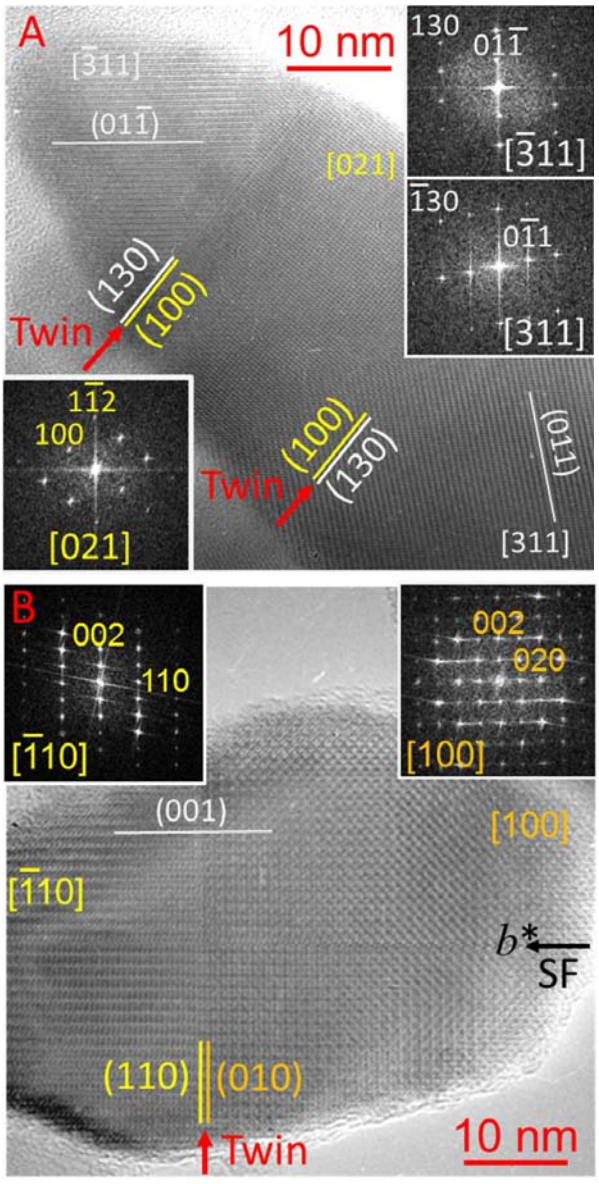

This is a preprint, the final version is subject to change, of the American Mineralogist (MSA)
Cite as Authors (Year) Title. American Mineralogist, in press.
(DOI will not work until issue is live.) DOI: http://dx.doi.org/10.2138/am-2017-5849

Fig. 7

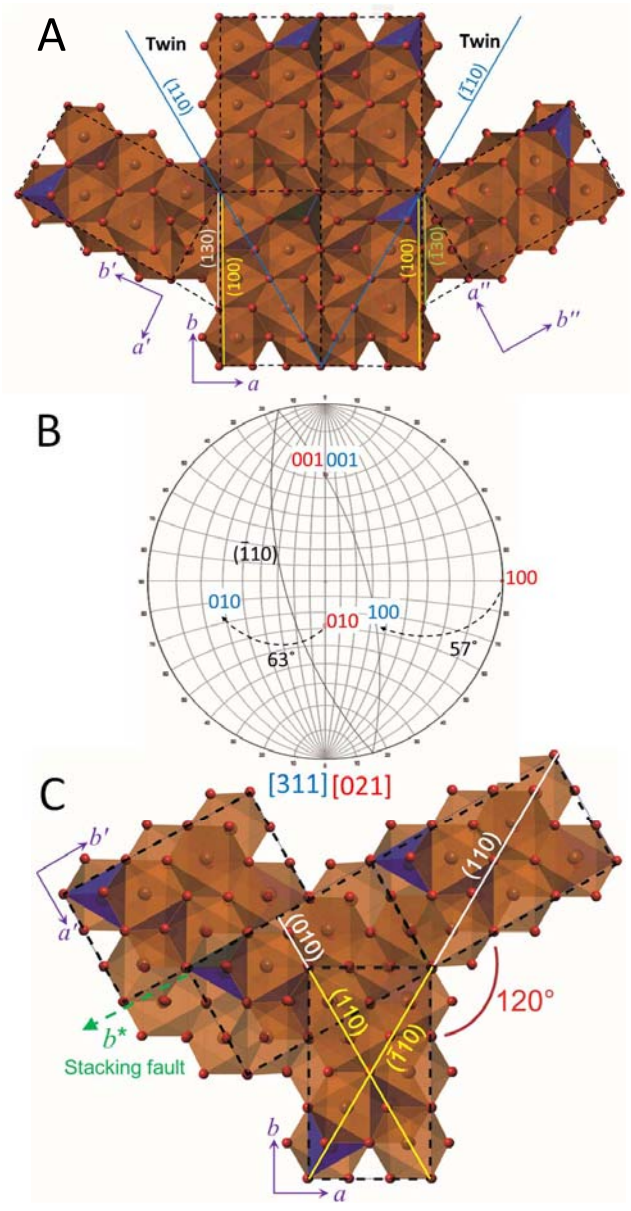

This is a preprint, the final version is subject to change, of the American Mineralogist (MSA)
Cite as Authors (Year) Title. American Mineralogist, in press.
(DOI will not work until issue is live.) DOI: http://dx.doi.org/10.2138/am-2017-5849

Fig. 8

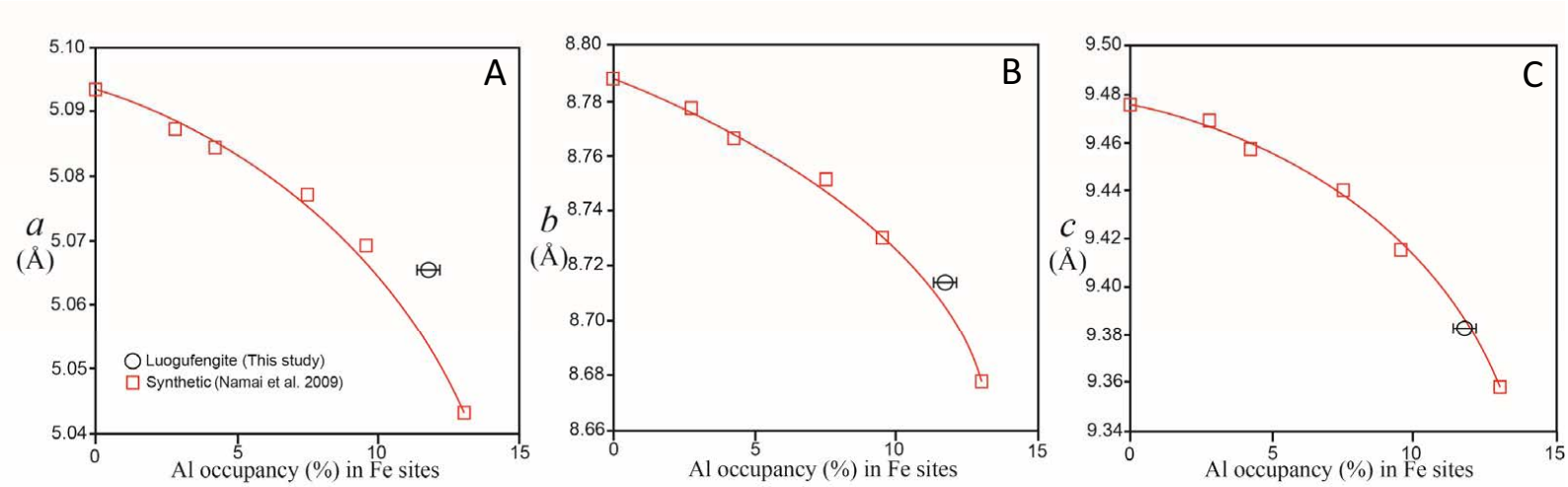

This is a preprint, the final version is subject to change, of the American Mineralogist (MSA)
Cite as Authors (Year) Title. American Mineralogist, in press.
(DOI will not work until issue is live.) DOI: http://dx.doi.org/10.2138/am-2017-5849

Fig. 9

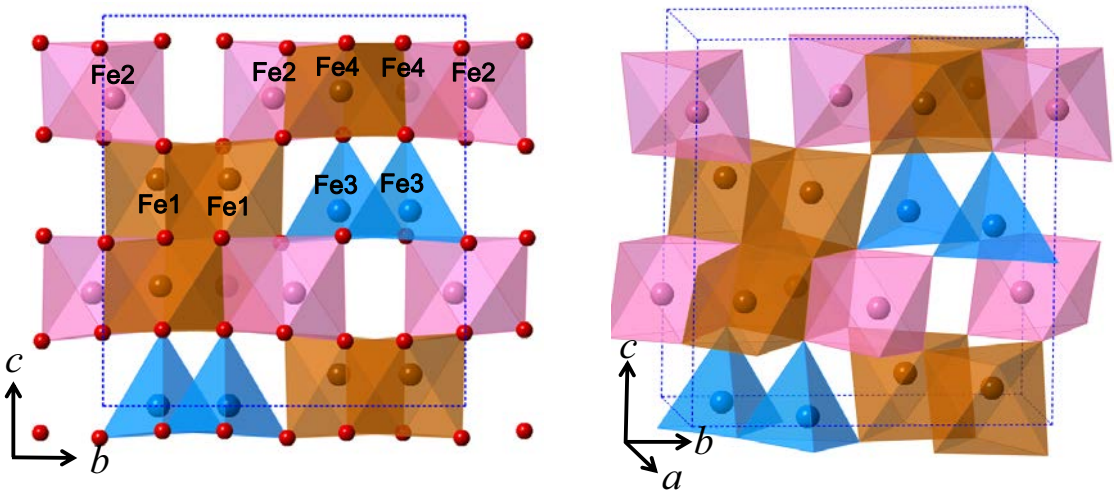

This is a preprint, the final version is subject to change, of the American Mineralogist (MSA)
Cite as Authors (Year) Title. American Mineralogist, in press.
(DOI will not work until issue is live.) DOI: http://dx.doi.org/10.2138/am-2017-5849

Fig. 10

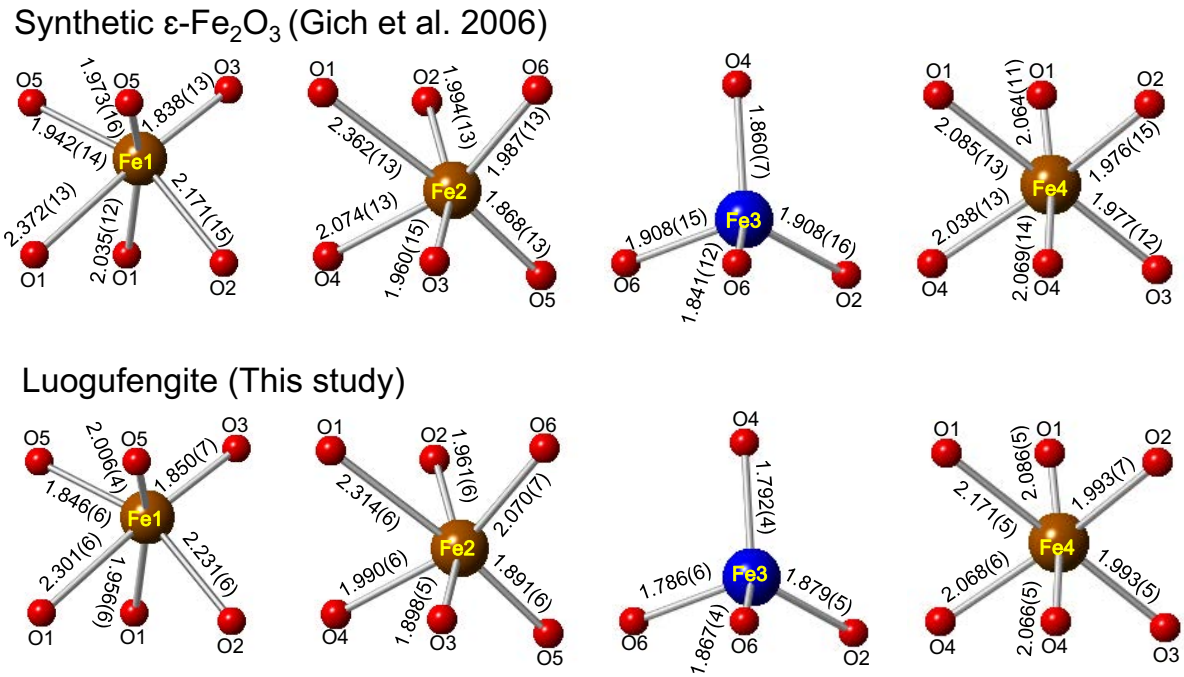

This is a preprint, the final version is subject to change, of the American Mineralogist (MSA)
Cite as Authors (Year) Title. American Mineralogist, in press.
(DOI will not work until issue is live.) DOI: http://dx.doi.org/10.2138/am-2017-5849

Fig. 11

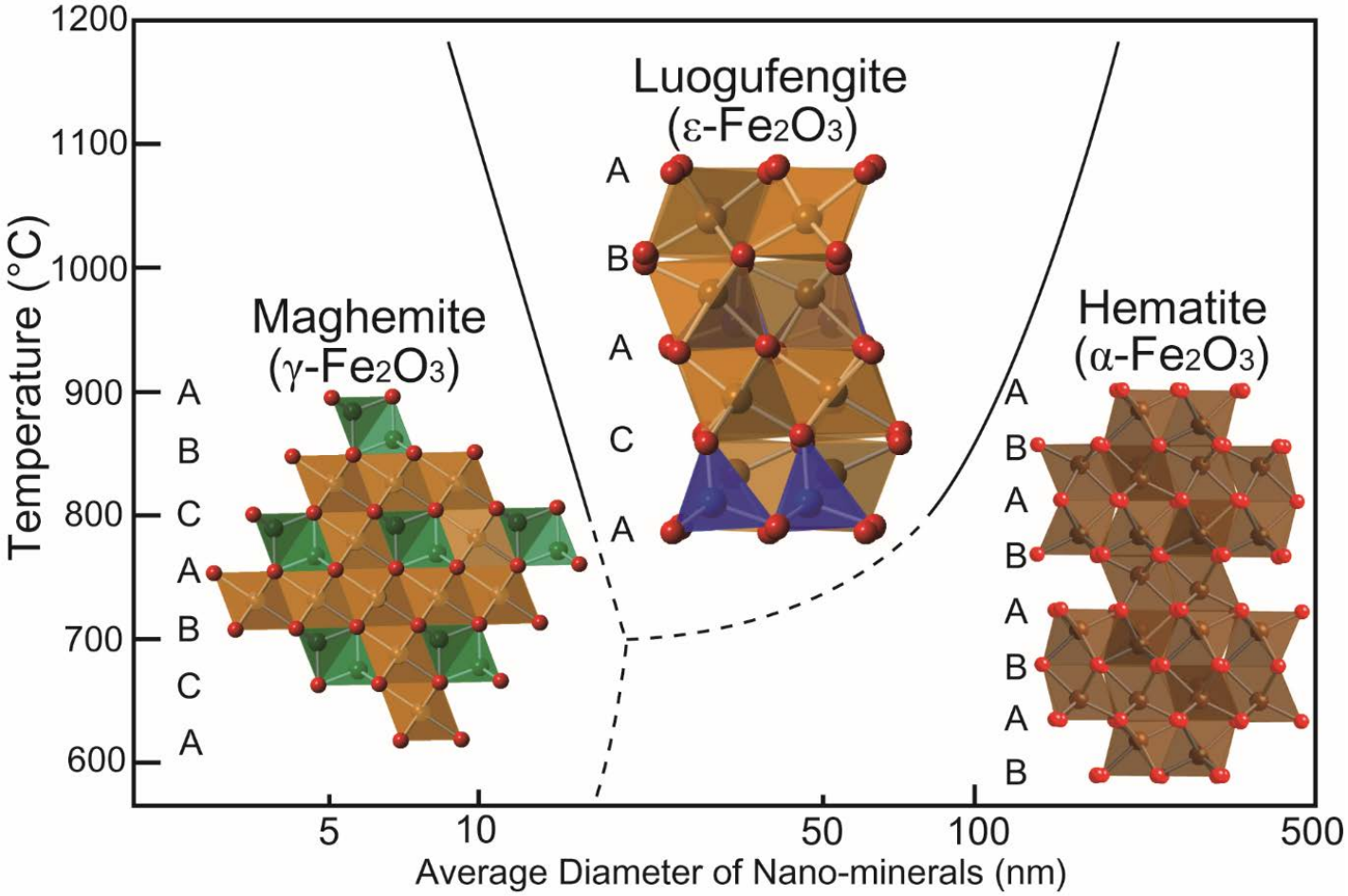

This is a preprint, the final version is subject to change, of the American Mineralogist (MSA)
Cite as Authors (Year) Title. American Mineralogist, in press.
(DOI will not work until issue is live.) DOI: http://dx.doi.org/10.2138/am-2017-5849

Fig. 12